Article

Cell Reports

Coordinated Regulation of Synaptic Plasticity at Striatopallidal and Striatonigral Neurons Orchestrates Motor Control

Graphical Abstract

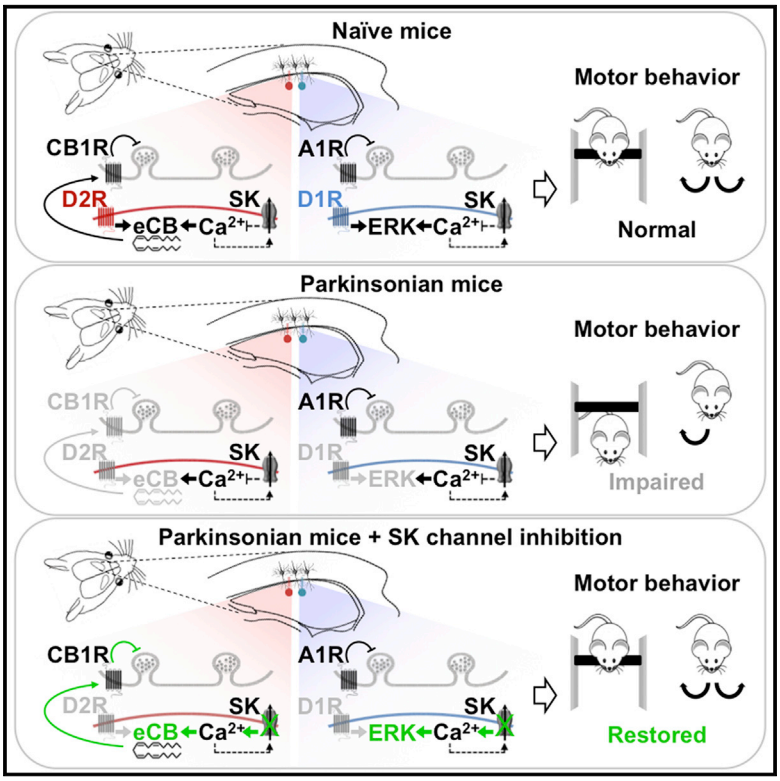

Highlights

- eCBs govern LTD in striatopallidal neurons and adenosine does so in striatonigral cells
- Parkinson's disease (PD)-like dopamine (DA) depletion impairs eCB-, but not adenosine-LTD
- DA deficits are circumvented by resuming cell-type-specific eCB and ERK signaling
- Segregated modulation of eCB and ERK signaling alleviates PD motor abnormalities

Authors

Massimo Trusel, Anna Cavaccini, Marta Gritti, ..., Ilaria Morella, Riccardo Brambilla, Raffaella Tonini

Correspondence

raffaella.tonini@iit.it

In Brief

Trusel et al. highlight the motor implications of restoring functional integration of presynaptic and postsynaptic mechanisms of plasticity at striatal projection neurons, by resuming cell-type-specific activation of eCB and ERK signaling in dopamine-depleted mice.

Trusel et al., 2015, Cell Reports *13*, 1353–1365
November 17, 2015
http://dx.doi.org/10.1016/j.celrep.2015.10.009

CellPress

Cell Reports
Article

Coordinated Regulation of Synaptic Plasticity at Striatopallidal and Striatonigral Neurons Orchestrates Motor Control

Massimo Trusel,[1,6] Anna Cavaccini,[1,6] Marta Gritti,[1,2] Barbara Greco,[1] Pierre-Philippe Saintot,[1] Cristiano Nazzaro,[1] Milica Cerovic,[3,4] Ilaria Morella,[4,5] Riccardo Brambilla,[3,4] and Raffaella Tonini[1,*]
[1]Neuroscience and Brain Technologies Department, Istituto Italiano di Tecnologia, 16163 Genova, Italy
[2]Life Science Department, University of Milan, 20133 Milano, Italy
[3]IRCCS, Mario Negri Institute for Pharmacological Research, 20156 Milano, Italy
[4]Neuroscience and Mental Health Research Institute, Division of Neuroscience, School of Biosciences, Cardiff University, Cardiff CF10 3AX, UK
[5]Institute of Experimental Neurology, Division of Neuroscience, IRCCS San Raffaele Scientific Institute and University, 20132 Milano, Italy
[6]Co-first author
*Correspondence: raffaella.tonini@iit.it
http://dx.doi.org/10.1016/j.celrep.2015.10.009

SUMMARY

The basal ganglia play a critical role in shaping motor behavior. For this function, the activity of medium spiny neurons (MSNs) of the striatonigral and striatopallidal pathways must be integrated. It remains unclear whether the activity of the two pathways is primarily coordinated by synaptic plasticity mechanisms. Using a model of Parkinson's disease, we determined the circuit and behavioral effects of concurrently regulating cell-type-specific forms of corticostriatal long-term synaptic depression (LTD) by inhibiting small-conductance Ca^{2+}-activated K^+ channels (SKs) of the dorsolateral striatum. At striatopallidal synapses, SK channel inhibition rescued the disease-linked deficits in endocannabinoid (eCB)-dependent LTD. At striatonigral cells, inhibition of these channels counteracted a form of adenosine-mediated LTD by activating the ERK cascade. Interfering with eCB-, adenosine-, and ERK signaling in vivo alleviated motor abnormalities, which supports that synaptic modulation of striatal pathways affects behavior. Thus, our results establish a central role of coordinated synaptic plasticity at MSN subpopulations in motor control.

INTRODUCTION

The dorsal striatum nucleus (DS) of the basal ganglia plays a central role in the physiological control of action selection and motor function (Packard and Knowlton, 2002). Motor information originating from cortical inputs converges on the medium spiny neurons (MSNs) of the DS. These MSNs express either D1 dopamine receptor (D1R) or D2 dopamine receptor (D2R), constituting the striatonigral ($D1_{MSN}$) and striatopallidal ($D2_{MSN}$) projection pathways, respectively (Albin et al., 1989; Kreitzer, 2009).

Dopamine released by projections from the substantia nigra pars compacta oppositely affects synaptic transmission in $D1_{MSN}$ and $D2_{MSN}$, depending on which receptor subtype is activated. In $D1_{MSN}$, dopamine strengthens cortical synaptic connections through the positive regulation of NMDA receptors and activation of the extracellular-signal regulated kinase (ERK) pathway (Cerovic et al., 2013; Girault et al., 2007). These cellular events ultimately trigger synaptic long-term potentiation (LTP) of glutamatergic cortical afferents (Calabresi et al., 1992; Cerovic et al., 2015; Pascoli et al., 2012).

In contrast, in $D2_{MSN}$, dopamine contributes to the depression of cortical inputs by gating the biosynthesis and release of local lipid mediator endocannabinoids (eCBs) (Lerner and Kreitzer, 2012). The synthesis of eCBs is dependent on the activation of metabotropic receptors (e.g., D2R and mGluRs1/5) and elevation of cytosolic Ca^{2+} concentration (Lerner and Kreitzer, 2012; Uchigashima et al., 2007). The eCBs act as retrograde messengers by activating the presynaptic CB1 cannabinoid receptor (CB1R), which decreases the probability of glutamate release and leads to long-term synaptic depression (eCB-LTD) (Gerdeman et al., 2002; Kreitzer and Malenka, 2007; Nazzaro et al., 2012; Shen et al., 2008; Wang et al., 2006).

Dopamine and eCB-mediated control of excitatory synaptic inputs to the DS is disrupted in animal models of motor disorders, including Parkinson's disease (PD) (Tritsch and Sabatini, 2012). In fact, some of the synaptic alterations found in PD mouse models involve deficits in dopamine-dependent LTP and eCB-LTD at striatal excitatory synapses (Kreitzer and Malenka, 2007; Picconi et al., 2003; Shen et al., 2008). These synaptic dysfunctions could potentially contribute to the striatonigral hypoactivity and striatopallidal hyperactivity characterizing the pathology, and ultimately to its motor symptoms (Albin et al., 1989; Kreitzer and Malenka, 2007).

For appropriate motor control, the dynamic integration between $D1_{MSN}$ and $D2_{MSN}$ activity appears to be crucial (Cui

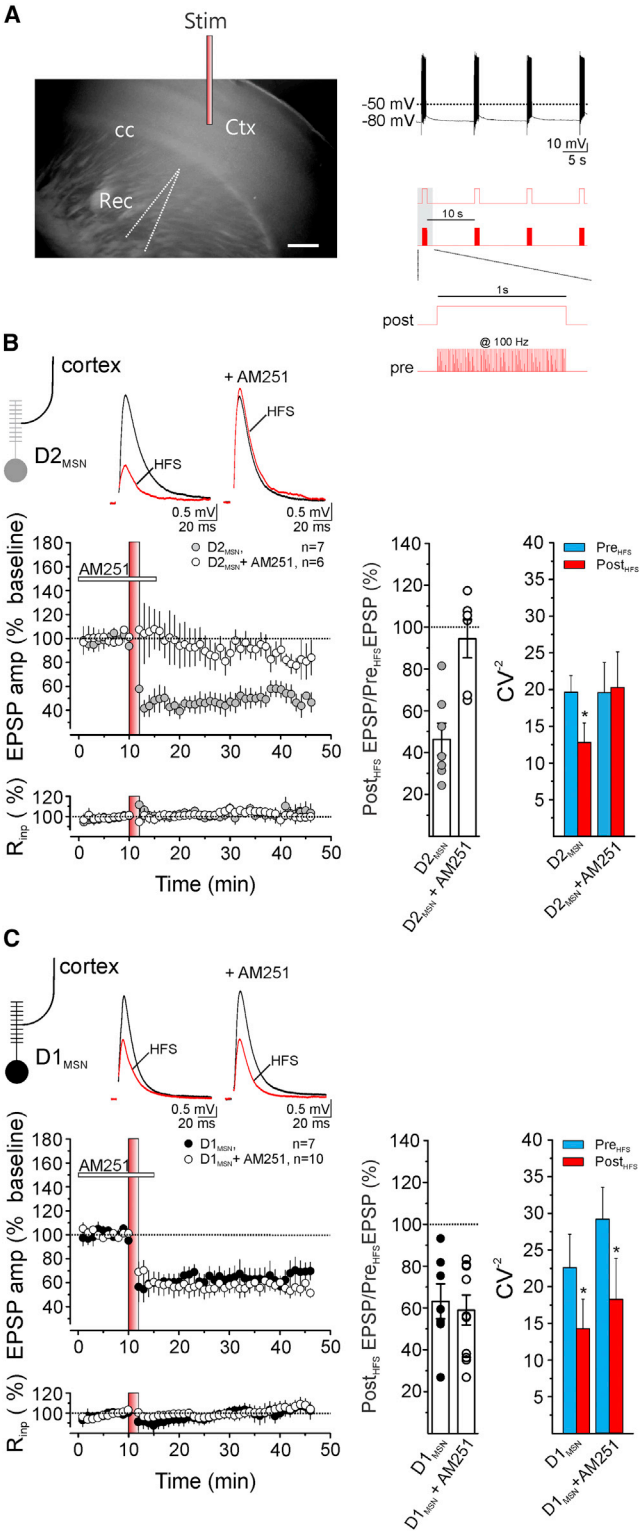

Figure 1. HFS-Induced LTD at Corticostriatal Afferents to $D2_{MSN}$ and $D1_{MSN}$

(A) (Left) Microphotograph of a horizontal slice displays the stimulation (Stim) and recording configuration (Rec) in the DLS. Ctx, cortex; cc, corpus callosum; scale bar, 300 μm. (Right) Postsynaptic response (black trace, top) to the HFS-pairing protocol for the induction of LTD (red trace, bottom) is shown.

(B and C) (Left) Time courses of normalized EPSP amplitude and normalized R_{inp} (mean ± SEM). (Insets) Averaged recordings (ten traces) before (black line) and after (red line) the delivery of the HFS protocol are shown. HFS stimulation is indicated by the red vertical bar. (Middle) Bar diagrams summarize the ratios of post-HFS and pre-HFS synaptic responses. (Right) Comparison of CV^{-2} before and after HFS delivery is shown ($D2_{MSN}$, $p = 0.03$; $D2_{MSN}$ + AM251, $p = 0.9$; $D1_{MSN}$, $p = 0.04$; $D1_{MSN}$ + AM251, $p = 0.02$; paired t test:). CV^{-2} calculations were based on 60 sweeps at 10 min before and 20 min after HFS. (B) LTD at cortical connections to $D2_{MSN}$ was abolished by the CB1R antagonist AM251 (4 μM; RM2W, $F_{1,11} = 17$, $p = 0.0014$; $D2_{MSN}$ versus $D2_{MSN}$ + AM251, $p < 0.01$, Bonferroni). (C) LTD at cortical connections to $D1_{MSN}$ was insensitive to CB1R antagonism (RM2W, $F_{1,15} = 0.1$, $p = 0.76$; $D1_{MSN}$ versus $D1_{MSN}$ + AM251).

et al., 2013; Tecuapetla et al., 2014), and loss of dopaminergic neurotransmission might cause abnormal coordination between the two projection pathways (Calabresi et al., 2014). However, the precise cellular mechanisms shaping the coordinated activity of $D1_{MSN}$ and $D2_{MSN}$ have yet to be established. We hypothesize that the two pathways may be coordinated through concurrent, cell-type-specific regulation of corticostriatal synaptic plasticity at $D1_{MSN}$ and $D2_{MSN}$. The loss of this regulation could disrupt motor control, leading to PD motor deficits.

To begin to address these hypotheses, we sought to identify the key presynaptic mechanisms that cooperate with postsynaptic dopaminergic signaling to regulate cell-type-specific forms of LTD at cortical connections to $D1_{MSN}$ and $D2_{MSN}$. We then investigated whether this functional interplay of presynaptic and postsynaptic molecular determinants of synaptic plasticity is lost in a mouse model of PD (the unilateral 6-hydroxydopamine [6-OHDA]-lesioned mouse).

We further examined whether it is possible to rescue PD motor deficits by mimicking the effect of postsynaptic dopaminergic regulation of plasticity by activating Ca^{2+}-dependent intracellular signaling cascades that act downstream of D2 and D1 dopamine receptors. In PD mice, bypassing dopamine signaling rescues disease-linked deficits in eCB-LTD in $D2_{MSN}$, and it counteracts a form of adenosine-mediated LTD in $D1_{MSN}$ by activating the postsynaptic ERK cascade. Activating eCB and ERK signaling in vivo alleviates specific motor abnormalities, improving motor control. These results establish that coordinated regulation of synaptic plasticity at striatal MSN subpopulations plays a major role in the control of motor function and in motor pathology.

RESULTS

Corticostriatal LTD in $D2_{MSN}$ and $D1_{MSN}$ Is Regulated by Different Mechanisms

To study synaptic plasticity at cortical connections to $D2_{MSN}$ and $D1_{MSN}$ of the dorsolateral striatum (DLS), we recorded evoked excitatory postsynaptic potentials (EPSPs) in physiological K^+-based intracellular conditions (high K^+), upon stimulation of the deep cortical layer V of the somatosensory cortex (Figure 1). $D2_{MSN}$ and $D1_{MSN}$ were identified by their negative resting membrane potentials ($D2_{MSN}$, −81 ± 0.4 mV, n = 62; $D1_{MSN}$, −80 ± 0.3 mV, n = 69), firing activity (Figure S1A; Kreitzer and Malenka,

2007), and after recording by immunostaining for adenosine A2A receptor (A2AR, for $D2_{MSN}$) and substance P (SP, for $D1_{MSN}$) (Figure S1B).

At cortical connections to $D2_{MSN}$, high-frequency stimulation (HFS) (Figure 1A) resulted in LTD of postsynaptic responses (49% ± 7% of baseline, n = 7; $p < 0.05$; Figure 1B). This plasticity is dependent on eCB signaling, as it was blocked by the CB1R antagonist AM251 (4 μM) (93% ± 9% of baseline, n = 6; $p > 0.05$; Figure 1B). In $D1_{MSN}$, the same HFS protocol also triggered a long-term depression (HFS-LTD) of EPSPs (60% ± 9% of baseline, n = 7; $p < 0.05$; Figure 1C). However, in $D1_{MSN}$, the HFS-LTD was unchanged by inhibiting CB1R (57% ± 7% of baseline, n = 10; $p < 0.05$; Figure 1C).

The plasticity in both $D2_{MSN}$ and $D1_{MSN}$ was associated with changes in the coefficient of variation (CV) of individual evoked EPSP after HFS, as reflected by the decreased CV^{-2} (CV^{-2} for $D2_{MSN}$, before: 20 ± 2, after: 13 ± 3, n = 6, $p < 0.05$; CV^{-2} for $D1_{MSN}$, before: 22 ± 5, after: 14 ± 4, n = 5, $p < 0.05$; Figures 1B and 1C). This result suggests a presynaptic locus of plasticity (Fino et al., 2005) in both populations. HFS-induced changes of CV^{-2} were abolished by AM251 selectively in $D2_{MSN}$, (CV^{-2} for $D2_{MSN}$, before: 20 ± 4, after: 20 ± 5, n = 6, $p > 0.05$; CV^{-2} for $D1_{MSN}$, before: 32 ± 5, after: 17 ± 5, n = 8, $p < 0.05$), supporting that activation of presynaptic CB1R mediates LTD at cortical connections to $D2_{MSN}$ (Kreitzer and Malenka, 2007; Nazzaro et al., 2012). To confirm this, we interfered with postsynaptic production of eCBs by targeting the enzymes phospholipase C-β (PLCβ) and phospholipase D (PLD), which participate in eCB biosynthesis in MSNs following HFS (Lerner and Kreitzer, 2012). The combined intracellular application of the PLCβ inhibitor U73122 (1 μM) and the PLD inhibitor CAY10594 (100 μM) fully prevented eCB-LTD in $D2_{MSN}$ (94% ± 9% of baseline, n = 5; $p > 0.05$; Figure 2A), but not in $D1_{MSN}$ (54% ± 11% of baseline, n = 6; $p < 0.05$; Figure 2D). Consistent with previous observations (Lerner and Kreitzer, 2012), inhibiting PLD alone was sufficient to impair plasticity at $D2_{MSN}$ synapses ($D2_{MSN}$, 95% ± 9% of baseline, n = 7; $p > 0.05$; Figure 2A). The same manipulation had no effect on $D1_{MSN}$ ($D1_{MSN}$, 52% ± 11% of baseline, n = 5; $p < 0.05$; Figure 2D). Taken together, these results demonstrate that eCB-mediated plasticity shows a bias toward cortico-$D2_{MSN}$ afferents.

The enzymatic activities of PLCβ and PLD and the biosynthesis of eCBs are stimulated by elevation of intracellular Ca^{2+} (Gerdeman et al., 2002; Lerner and Kreitzer, 2012). Including the calcium chelator BABTA (20 mM) in the postsynaptic neurons prevented LTD at $D2_{MSN}$ synapses (97% ± 8% of baseline, n = 6; $p > 0.05$; Figure 2B), but not in $D1_{MSN}$ (48% ± 11% of baseline, n = 5; $p < 0.05$; Figure 2E). This is further evidence that cortically induced LTD is driven by different mechanisms in $D2_{MSN}$ and $D1_{MSN}$.

Our data indicating that eCBs do not gate HFS-induced LTD at $D1_{MSN}$ synapses agree with some previous studies (Kreitzer and Malenka, 2007; Nazzaro et al., 2012), but contradict others (Bagetta et al., 2011; Wang et al., 2006). We therefore asked whether $D1_{MSN}$ could express a form of eCB-dependent LTD when the postsynaptic biosynthesis of eCBs is facilitated, such as upon stimulation of mGlurR1/5 (Uchigashima et al., 2007). To test this, we measured changes in the amplitude of EPSPs at cortical synapses in $D2_{MSN}$ and $D1_{MSN}$ after application of the mGlurR1/5 agonist DHPG (100 μM; postsynaptic neuron held at −60 mV; Figure S2). We found that DHPG triggered a form of synaptic depression ($D2_{MSN}$, 61% ± 8% of baseline, n = 8; $p < 0.05$; $D1_{MSN}$, 71% ± 6% of baseline, n = 10; $p < 0.05$) that was sensitive to the CB1R antagonist AM251 (4 μM) in both neuronal subpopulations ($D2_{MSN}$, 91% ± 6% of baseline, n = 6; $p > 0.05$; $D1_{MSN}$, 91% ± 2% of baseline, n = 7; $p > 0.05$; Figures S2A and S2B).

Overall, these results indicate that HFS-LTD at cortical afferents to $D1_{MSN}$ is not primarily gated by eCBs, which can, however, be released to depress cortical inputs in response to the direct pharmacological activation of mGlur1/5R.

Dopamine Signaling Modulates LTD Oppositely in $D2_{MSN}$ and $D1_{MSN}$

We next investigated how dopamine signaling modulates LTD in the two MSN subpopulations. Previous studies have indicated that LTD obtained by stimulation of excitatory afferents to the striatum requires the activation of D2R in both $D2_{MSN}$ and $D1_{MSN}$ (Bagetta et al., 2011; Wang et al., 2006). To test whether this was the case in our experimental setting, we treated slices with the D2R antagonist sulpiride (10 μM). Under these conditions, LTD was impaired at cortical connections to $D2_{MSN}$ (85% ± 5% of baseline, n = 6; $p > 0.05$; Figure 2C), consistent with the contribution of D2 signaling to eCB biosynthesis upon HFS (Lerner and Kreitzer, 2012). Conversely, HFS-LTD at cortical afferents on $D1_{MSN}$ was not affected by inhibiting D2R ($D1_{MSN}$, 50% ± 5% of baseline, n = 8; $p < 0.05$; Figure 2F).

In $D1_{MSN}$, postsynaptic D1R activation positively regulates the NMDA receptor and ERK signaling cascade, thus increasing synaptic responsiveness to cortical inputs (Cahill et al., 2014; Cerovic et al., 2013; Girault et al., 2007). It is, therefore, possible that D1R activation hinders HFS-LTD in $D1_{MSN}$. This is indeed the case, as the D1R agonist SKF38393 (3 μM) markedly reduced LTD at cortical connections to $D1_{MSN}$ (88% ± 6% of baseline, n = 6; $p > 0.05$; Figure 2F).

Collectively, our data indicate that postsynaptic dopaminergic signaling downstream of D2R in $D2_{MSN}$ and D1R in $D1_{MSN}$ oppositely regulates LTD.

Adenosine Mediates HFS-LTD in $D1_{MSN}$

To elucidate the mechanisms underlying the induction of LTD by HFS in $D1_{MSN}$, we tested the involvement of distinct classes of presynaptic receptors that could regulate the release of glutamate at corticostriatal afferents. In other brain regions, the activation of presynaptic NMDA receptors (NMDARs) can trigger a long-lasting depression of glutamatergic neurotransmission (Min and Nevian, 2012). This was not the case in the DS, as HFS-LTD in $D1_{MSN}$ was unaffected by the NMDAR antagonist DL-APV (50 μM; 56% ± 12% of baseline, n = 5; $p < 0.05$; Figure 3A). The presynaptic group 2-metabotropic glutamate receptors (mGluR2/3) have been shown to induce pharmacological LTD at excitatory striatal synapses (Kupferschmidt and Lovinger, 2015). However, the selective mGlur2/3 antagonist LY341495 (200 nM) did not prevent LTD upon HFS in $D1_{MSN}$ (58% ± 5% of baseline, n = 5; $p < 0.05$; Figure 3B).

A1 adenosine receptors (A1Rs) have been identified at striatal glutamatergic terminals, where they can negatively modulate

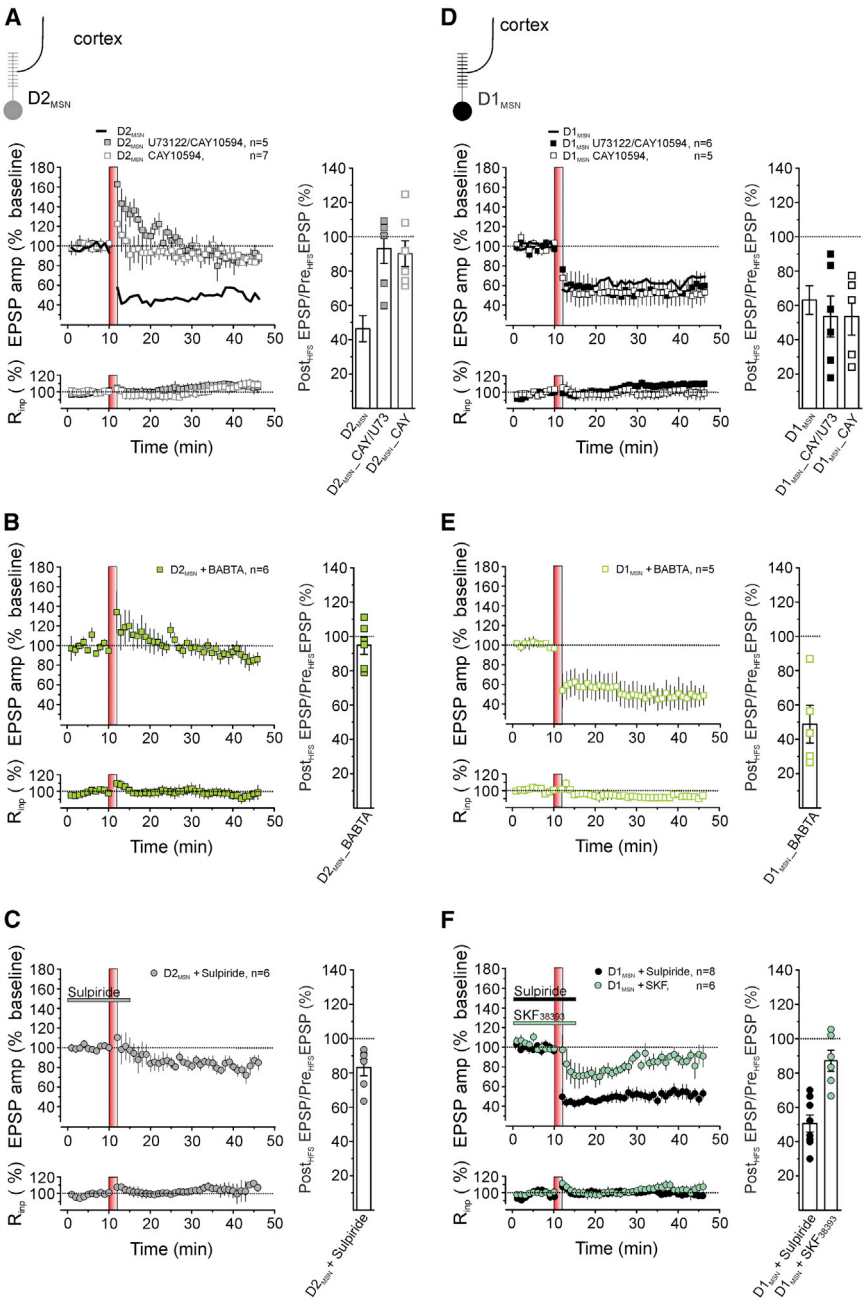

Figure 2. Modulation of HFS-LTD at Cortical Connections to $D2_{MSN}$ and $D1_{MSN}$

(A and D) The combined intracellular application of the PLCβ inhibitor U73122 (1 μM) and PLD inhibitor CAY10594 (100 μM) prevented LTD induction in $D2_{MSN}$ (A), but not in $D1_{MSN}$ (D). Similar results were obtained when CAY10594 was applied in isolation (A; RM2W, $F_{2,16}$ = 12, p = 0.0007; $D2_{MSN}$ + U73122/CAY10594 versus $D2_{MSN}$, p < 0.01; $D2_{MSN}$ + CAY10594 versus $D2_{MSN}$, p < 0.001, Bonferroni; D; 2WRM, $F_{2,15}$ = 0.15, p = 0.9).

(B and E) Intracellular application of the Ca^{2+} chelator BABTA (20 mM) inhibited LTD in $D2_{MSN}$ (B; RM2W, $F_{1,11}$ = 39.2, p < 0.001; $D2_{MSN}$ BABTA versus $D2_{MSN}$, p < 0.001, Bonferroni), but not in $D1_{MSN}$ (E; RM2W, $F_{1,10}$ = 0.69, p = 0.43; $D1_{MSN}$ BABTA versus $D1_{MSN}$).

(C and F) eCB-LTD and HFS-LTD showed differences in sensitivity to bath application of the D2 receptor antagonist sulpiride (10 μM; **C**; $D2_{MSN}$, gray bar; F; $D1_{MSN}$, black bar). Compared to control conditions (Figures 1B and 1C), sulpiride reduced eCB-LTD at cortical connections to $D2_{MSN}$ (C; RM2W, $F_{1,11}$ = 20, p = 0.001; $D2_{MSN}$ + sulpiride versus $D2_{MSN}$, p < 0.01, Bonferroni), but failed to inhibit HFS-LTD at cortical afferents on $D1_{MSN}$ (F; RM2W, $F_{1,13}$ = 0.6, p = 0.4; $D1_{MSN}$ + sulpiride versus $D1_{MSN}$). (F) D1R activation negatively modulated HFS-LTD at $D1_{MSN}$ synapses (RM2W, $F_{2,18}$ = 8, p = 0.003; $D1_{MSN}$ +SKF versus $D1_{MSN}$, p < 0.05; $D1_{MSN}$ +SKF versus $D1_{MSN}$ + sulpiride, p < 0.01, Bonferroni).

(A and F) (Left) Data are presented as normalized EPSP amplitude and normalized R_{inp} (mean ± SEM). Black line shows eCB-LTD in $D2_{MSN}$ (A) and HFS-LTD in $D1_{MSN}$ (D) from Figures 1B and 1C, respectively, measured under control conditions and reported here for reference. (Right) Bar diagrams summare the ratios of post-HFS and pre-HFS synaptic responses.

glutamate release (Borycz et al., 2007). To test whether A1Rs contribute to cell-type-specific synaptic plasticity at striatal circuits, we delivered HFS in the presence of the selective A1R antagonist DPCPX (500 nM). Inhibition of A1R abolished LTD in $D1_{MSN}$ (94% ± 5% of baseline, n = 13; p > 0.05; Figure 3C), but not in $D2_{MSN}$ (49% ± 7% of baseline, n = 6; p < 0.05; Figure S3). DPCPX alone had no effect on basal glutamatergic synaptic transmission in either neuronal subpopulation ($D1_{MSN}$, 101% ± 5% of baseline, n = 10, p > 0.05; $D2_{MSN}$, 104% ± 6% of baseline, n = 6, p > 0.05, data not shown). This indicates a lack of tonic inhibition by extracellular adenosine, which is most likely released in response to HFS of cortical afferents. A second A1R antagonist, CPT (200 nM), also blocked LTD at $D1_{MSN}$ (91% ± 6% of baseline, n = 6; p > 0.05; Figure 3C).

We next tested the effect of the selective A1R agonist 5′-Chloro-5′-deoxy-(±)-ENBA (ENBA, 200 nM) on synaptic transmission at cortical connections to $D1_{MSN}$. Activation of A1R produced a persistent depression of synaptic responses generated by twin cortical stimuli (p1, 53% ± 14% of baseline; p < 0.05; Figure 3D). This synaptic depression was rescued by the A1R antagonist DPCPX (500 nM; p1, 82% ± 15% of baseline, n = 5; p > 0.05; Figure 3D). Like LTD triggered by HFS (Figure 1C), the ENBA-induced LTD was expressed presynaptically, as indicated by the increased paired-pulse ratio (PPR) of synaptic responses that reversed upon DPCPX application (PPR: baseline, 0.9 ± 0.07; ENBA, 1.7 ± 0.2; DPCPX, 1.13 ± 0.1; **p < 0.01; *p < 0.05; Figure 3D). Collectively, these results suggest that adenosine triggers a

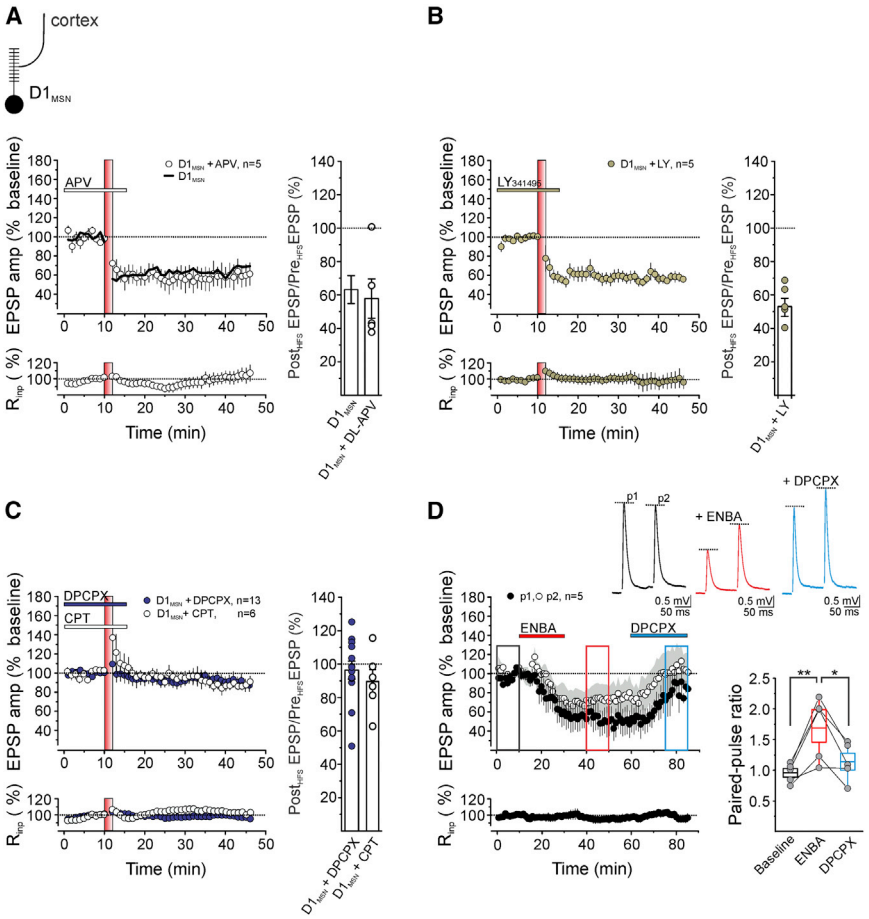

Figure 3. Adenosine A1 Receptor Mediates LTD in $D1_{MSN}$

(A–C) (Left) Time courses of normalized EPSP amplitude and normalized R_{inp} (mean ± SEM). (Right) Bar diagrams summarize the ratios of post-HFS and pre-HFS synaptic responses. Synaptic plasticity at cortical connections to $D1_{MSN}$ is shown. Bath application of the NMDA receptor antagonist DL-APV (A, 50 μM, white bar) and mGlur2/3 antagonist LY341495 (B, 200 nM, gray bar) did not affect plasticity of EPSPs compared to the control conditions shown in Figure 1C (RM2W, $F_{1,10} = 0.03$ p = 0.86, $D1_{MSN}$ + APV versus $D1_{MSN}$; $F_{1,10} = 0.04$, p = 0.84, $D1_{MSN}$ + LY341495 versus $D1_{MSN}$). Black line in (A) shows HFS-LTD in $D1_{MSN}$ from Figure 1C. (C) Bath application of the A1R antagonists DPCPX (500 nM, blue bar) or CPT (200 nM, white bar) prevented HFS-LTD of EPSPs in $D1_{MSN}$ (RM2W, $F_{2,23} = 8$, p = 0.003, $D1_{MSN}$ + DPCPX versus $D1_{MSN}$, p < 0.01; $D1_{MSN}$ + CPT versus $D1_{MSN}$, p < 0.05; $D1_{MSN}$ + DPCPX versus $D1_{MSN}$ + CPT, p = 1, Bonferroni).

(D) Pharmacological A1R-mediated LTD at cortical connections to $D1_{MSN}$. (Left) Time course (mean ± SEM) of the first peak (p1) and second peak (p2) amplitudes of synaptic responses generated by twin stimuli at a 100-ms interval. The A1R agonist ENBA (200 nM, red bar) triggered a depression of EPSPs that was rescued by the A1R antagonist DPCPX (500 nM, blue bar; at the time points indicated in the time course, baseline versus ENBA p < 0.05; baseline versus DPCPX p > 0.05, RM1W, Tukey). The gray area represents SEM values for p2. (Right) Box-chart diagram indicates the PPRs of baseline (black box), ENBA (red box), and DPCPX (blue box) at the time points indicated in the time course. The values represented are the minimum, mean (bar inside the box), and the maximum. ENBA-induced LTD was associated with increased PPR that reversed upon DPCPX application (baseline versus ENBA p < 0.01; ENBA versus DPCPX p < 0.05, RM1W, Tukey). (Insets) Averaged recordings (ten traces) before (black) and after the application of ENBA (red) or DPCPX (blue). PPR was expressed as the ratio between the amplitude of the second and the first EPSPs.

form of HFS-LTD at cortico-$D1_{MSN}$ synapses that requires the activation of presynaptic A1R.

In summary, in response to cortical stimulation, LTD at connections to $D2_{MSN}$ requires the activation of CB1R and D2R, whereas HFS-LTD at connections to $D1_{MSN}$ does not. HFS-LTD in $D1_{MSN}$ is instead reduced when postsynaptic D1R is co-activated and is dependent on presynaptic A1R. Postsynaptic dopaminergic signaling thus influences these two forms of LTD in opposite ways. That is, in $D2_{MSN}$, intracellular cascades downstream of D2R could facilitate the induction of eCB-LTD by promoting eCB biosynthesis (Lerner and Kreitzer, 2012). In $D1_{MSN}$, activation of signaling cascades downstream of D1R could dynamically suppress LTD by counteracting the effect of presynaptic A1R that reduces glutamate release.

Corticostriatal LTD in $D2_{MSN}$ and $D1_{MSN}$ of 6-OHDA-Lesioned Mice

This cell-type-specific, dopaminergic regulation of LTDs may be lost upon dopaminergic denervation in PD. In this case, at cortical synapses to $D2_{MSN}$ in the disease state, D2R would not contribute to eCB biosynthesis, and eCB-LTD would be impaired (Lerner and Kreitzer, 2012). In contrast, at cortical synapses to $D1_{MSN}$, presynaptic induction mechanisms of A1R-mediated LTD would be unaffected. What might be lost in vivo is the antagonist interaction between presynaptic A1R- and postsynaptic D1-mediated signaling in modulating the strength of cortical inputs. Together, these pathway-specific effects might lead to dysfunctional integration of $D2_{MSN}$ and $D1_{MSN}$ activity and, ultimately, to motor deficits.

As a first step to test these hypotheses, we examined corticostriatal synaptic plasticity in the unilateral 6-OHDA-lesioned mouse model of PD (Schwarting and Huston, 1996). Upon HFS, LTD was indeed impaired at cortical connections to $D2_{MSN}$ in 6-OHDA-lesioned mice (6-OHDA_{ipsi}, 91% ± 5% of baseline, n = 9; p > 0.05; Figure 4A) compared to sham animals ($Sham_{ipsi}$, 52% ± 8% of baseline, n = 5; p < 0.05; Figure 4A). These results are consistent with previous studies showing the loss of eCB-mediated LTD in $D2_{MSN}$ of 6-OHDA mice upon intrastriatal HFS of excitatory terminals (Kreitzer and Malenka, 2007; Lerner and Kreitzer, 2012). In contrast, in $D1_{MSN}$ of 6-OHDA- and sham-lesioned mice, HFS-LTD was of comparable magnitude (6-OHDA_{ipsi}, 61% ± 7% of baseline, n = 11, p < 0.05; $Sham_{ipsi}$, 65% ± 7% of baseline, n = 5, p < 0.05; Figure 4B).

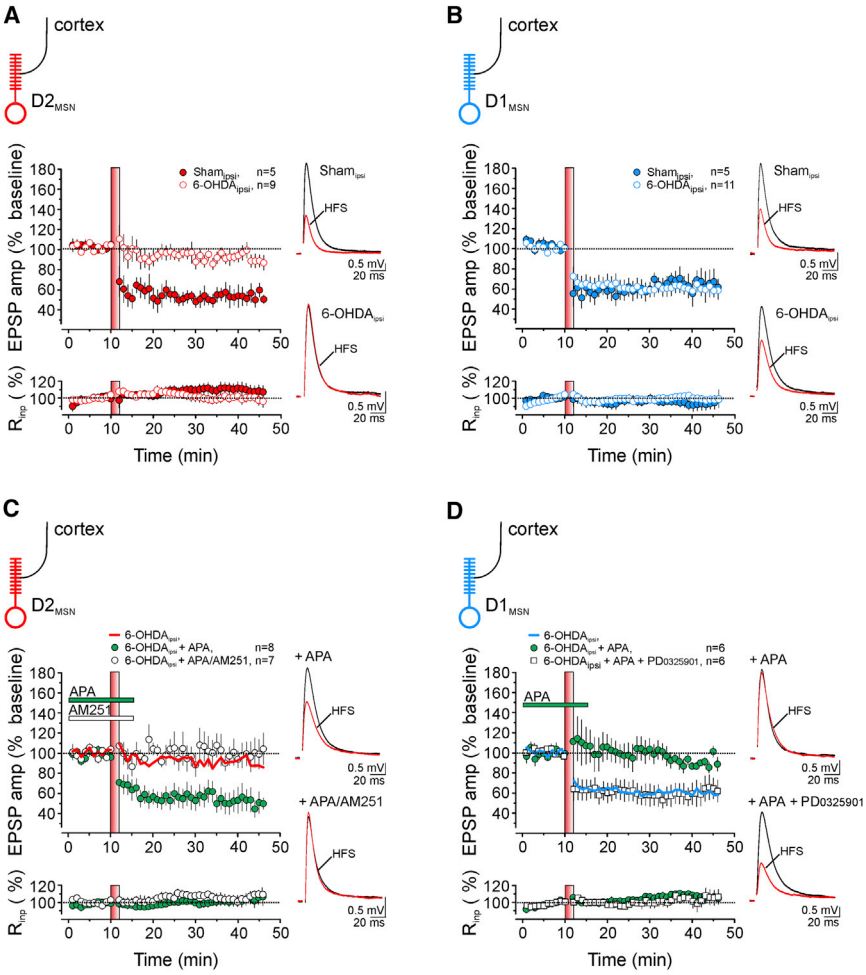

Figure 4. SK Channel Inhibition Dichotomously Modulates Corticostriatal LTD at $D2_{MSN}$ and $D1_{MSN}$ Synapses of 6-OHDA-Lesioned Mice

(A) Upon dopamine depletion, LTD was impaired at glutamatergic synapses of $D2_{MSN}$ 6-OHDA mice compared to sham animals (RM2W, $F_{1,12}$ = 20, p = 0.0007; $D2_{MSN}$ 6-$OHDA_{ipsi}$ versus $D2_{MSN}$ $Sham_{ipsi}$, p < 0.01, Bonferroni).

(B) In contrast, induction of HFS-LTD was unaffected in $D1_{MSN}$ 6-OHDA mice (RM2W, $F_{1,14}$ = 0.8, p = 0.39, $D1_{MSN}$ 6-$OHDA_{ipsi}$ versus $D1_{MSN}$ $Sham_{ipsi}$).

(C) Bath application of the SK channel inhibitor apamin (100 nM, green bar) reinstated a form of LTD at $D2_{MSN}$ synapses of 6-OHDA-lesioned mice, which was sensitive to the CB1R antagonist AM251 (4 μM, white bar; RM2W, $F_{2,21}$ = 7.3, p = 0.0038; $D2_{MSN}$ 6-$OHDA_{ipsi}$ + APA versus $D2_{MSN}$ 6-$OHDA_{ipsi}$, p < 0.05; $D2_{MSN}$ 6-$OHDA_{ipsi}$ + APA versus $D2_{MSN}$ 6-$OHDA_{ipsi}$ + APA/AM251, p < 0.01; $D2_{MSN}$ 6-$OHDA_{ipsi}$ + APA/AM251 versus $D2_{MSN}$ 6-$OHDA_{ipsi}$, p = 1, Bonferroni). Red line shows eCB-LTD in $D2_{MSN}$ 6-OHDA mice, as reported in (A).

(D) Exposure to apamin abolished HFS-LTD in $D1_{MSN}$ 6-$OHDA_{ipsi}$ mice. This effect was averted by including the MEK/ERK inhibitor PD0325901 (20 nM) in the postsynaptic neuron (RM2W, $F_{2,20}$ = 12, p = 0.0003; $D1_{MSN}$ 6-$OHDA_{ipsi}$ + APA versus $D1_{MSN}$ 6-$OHDA_{ips}$, p < 0.001; $D1_{MSN}$ 6-$OHDA_{ipsi}$ + APA versus $D1_{MSN}$ 6-$OHDA_{ipsi}$ + APA + PD0325901, p < 0.01; $D1_{MSN}$ 6-$OHDA_{ipsi}$ + APA + PD0325901 versus $D1_{MSN}$ 6-$OHDA_{ipsi}$, p = 1, Bonferroni). Blue line indicates HFS-LTD in $D1_{MSN}$ 6-OHDA mice, as reported in (B).

Data are presented as normalized EPSP amplitude and normalized R_{inp} (mean ± SEM). Insets represent superimposed averaged recordings (ten traces) before (black line) and after (red line) the delivery of the HFS protocol.

Inhibition of SK Channel Activity Dichotomously Modulates LTD at Striatal Pathways in PD Model Mice

To determine whether PD motor deficits are directly linked to a dysfunctional coordination of presynaptic and postsynaptic mechanisms of plasticity at both striatal pathways, we designed a rescue experiment. First, we devised a method to recapitulate the postsynaptic regulation of eCB-LTD and A1R-LTD at striatal pathways in PD model mice, and then we assessed the effects of this rescue on motor behavior.

Activating Ca^{2+}-dependent intracellular signaling cascades that act downstream of D2 and D1 dopamine receptors would modulate the activity of the two pathways, bypassing the need for dopamine itself. For this purpose, we targeted the activity of the small-conductance Ca^{2+}-activated K^+ (SK) channels. Through negative feedback, inhibition of SK channel activity enhances Ca^{2+} signals triggered by back-propagating action potentials (Tonini et al., 2013) and by synaptic activation of NMDAR (Bloodgood and Sabatini, 2008) in several brain regions. This negative feedback also applies to the postsynaptic Ca^{2+} transients evoked by HFS stimulation of cortical afferents to $D2_{MSN}$ and $D1_{MSN}$ (Figure S4).

In $D2_{MSN}$, inhibition of SK channels facilitates the Ca^{2+}-dependent release of eCBs and eCB-LTD, bypassing the postsynaptic activation of D2R (Nazzaro et al., 2012). In $D1_{MSN}$, voltage-dependent Ca^{2+} influx activates the ERK signaling pathway and ERK-mediated plasticity (Cahill et al., 2014; Girault et al., 2007); the postsynaptic ERK cascade has been shown to increase the synaptic responsiveness of $D1_{MSN}$ (Cerovic et al., 2015; Pascoli et al., 2012). Inhibition of SK channel activity could be thus used to boost the activation of the ERK signaling pathway independent of D1R.

In this view, inhibition of SK channel activity should restore eCB-LTD in $D2_{MSN}$ and counteract LTD in $D1_{MSN}$ in 6-OHDA mice.

Indeed, bath application of the selective SK channel inhibitor apamin (APA, 100 nM) during HFS rescued LTD in $D2_{MSN}$ of 6-$OHDA_{ipsi}$ mice ($D2_{MSN}$ 6-$OHDA_{ipsi}$ + APA, 52% ± 11% of baseline, n = 8; p < 0.05; Figure 4C). The effect of apamin was mediated by the activation of CB1R, since applying the antagonist AM251 prevented the rescue ($D2_{MSN}$ 6-$OHDA_{ipsi}$ + APA/AM251, 97% ± 10% of baseline, n = 7; p > 0.05; Figure 4C).

Consistent with our hypothesis, SK channel inhibition at $D1_{MSN}$ 6-$OHDA_{ipsi}$ synapses had the opposite effect. In the presence of apamin, HFS did not result in LTD ($D1_{MSN}$ 6-$OHDA_{ipsi}$ + APA, 91% ± 5% of baseline, n = 6; p > 0.05; Figure 4D). Apamin's

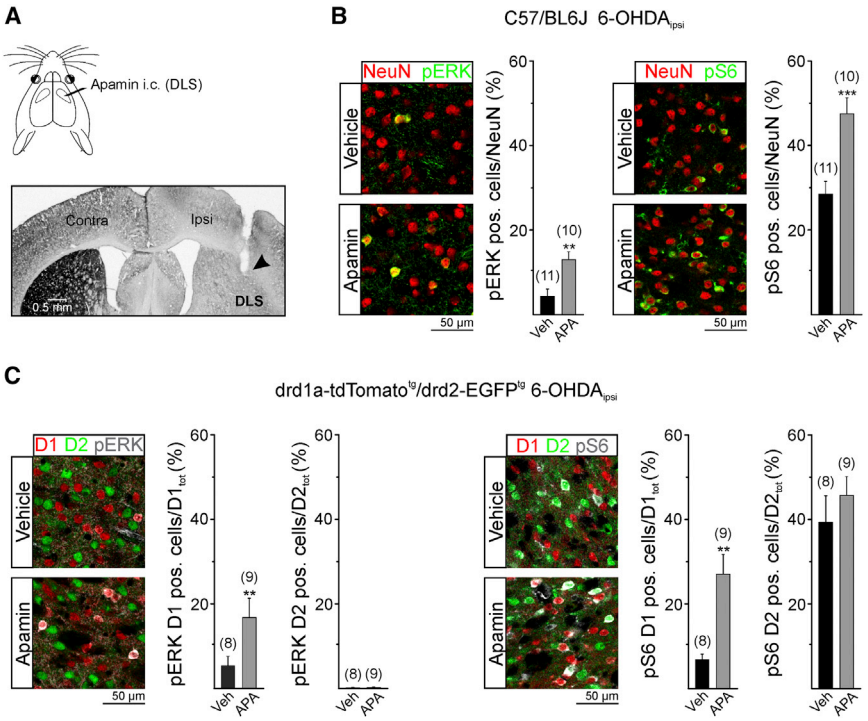

Figure 5. SK Channel Inhibition Selectively Potentiates the ERK Signaling Cascade in D1$_{MSN}$

(A) (Top) Schematic representation of the unilateral intracerebral (i.c.) injection of apamin (0.08 ng in 0.5 µl) or vehicle. (Bottom) Photomicrograph shows a TH-stained coronal section depicting the cannula track (marked by the arrowhead) within the ipsilateral DLS of a 6-OHDA-lesioned mouse. (B and C) Confocal laser scanning immunofluorescent detection of apamin-induced phosphorylation of ERK and protein S6 in the ipsilateral DLS of 6-OHDA-lesioned mice. (B) Representative images and quantification (mean ± SEM) of pERK- (left, green) and pS6- (right, green) positive cells in C57/Bl6J mice are shown (pERK, vehicle n = 11, apamin n = 10, $p < 0.01$, t test; pS6, vehicle n = 11, apamin n = 10, $p < 0.001$, t test). The neuronal marker NeuN is in red. (C) pERK- (left, gray) and pS6- (right, gray) positive cells in D1$_{MSN}$ and D2$_{MSN}$ of drd1a-tdTomato^{tg} (D1, red)/drd2-EGFP^{tg} (D2, green) mice are shown (vehicle n = 8, apamin n = 9; mean ± SEM). In the ipsilateral DLS of drd1a-tdTomato^{tg}/drd2-EGFP^{tg} mice infused with apamin or vehicle, two-way ANOVA, Bonferroni's post hoc test, revealed a significant effect of the treatment in D1$_{MSN}$, but not in D2$_{MSN}$ (pERK, $F_{1,30} = 5$, $p = 0.04$; D1$_{MSN}$, vehicle versus apamin $p < 0.01$; D2$_{MSN}$, vehicle versus apamin $p = 1$; pS6, $F_{1,30} = 8$, $p = 0.007$; D1$_{MSN}$, vehicle versus apamin $p < 0.01$; D2$_{MSN}$, vehicle versus apamin $p = 0.5$). Note the colocalization of pERK and pS6 and D1$_{MSN}$ (red) (***$p < 0.001$ and **$p < 0.01$).

effect was due to the activation of ERK signaling in the postsynaptic D1$_{MSN}$; including the MEK/ERK pathway inhibitor PD0325901 (20 nM) in the intracellular recording solution restored LTD in D1$_{MSN}$ (D1$_{MSN}$ 6-OHDA$_{ipsi}$ + APA/PD0325901, 69% ± 11% of baseline, n = 6; $p < 0.05$; Figure 4D). To further investigate how presynaptic mechanisms of LTD and postsynaptic ERK signaling interact in D1$_{MSN}$ of PD mice, we tested the effect of co-application of apamin with the A1R antagonist DPCPX. In D1$_{MSN}$ 6-OHDA$_{ipsi}$ neurons, this manipulation did not shift synaptic plasticity further toward LTP (D1$_{MSN}$ 6-OHDA$_{ipsi}$ + APA/DPCPX, 101% ± 7% of baseline, n = 7; $p > 0.05$; data not shown), possibly because of impaired molecular mechanisms underlying the expression of synaptic potentiation in PD mice (Calabresi et al., 2000; Picconi et al., 2003).

Collectively, these results suggest that, at D1$_{MSN}$ of PD mice, SK channel inhibition counteracts LTD by promoting ERK cascade activation.

Inhibition of SK Channel Activity In Vivo Specifically Activates ERK Signaling in D1$_{MSN}$

To confirm that SK channel modulation affects ERK signaling in striatal circuits and to test whether this effect is cell-type specific, we administered apamin in vivo. We infused either apamin (0.08 ng/0.5 µl intracerebrally [i.c.]) or saline in the ipsilateral DLS of 6-OHDA-lesioned mice (Figure 5A). After 10 min, we monitored phosphorylation of both ERK1/2 and the downstream target ribosomal protein S6 at Ser235/236, a site known to be a direct target of activated ERK (Cerovic et al., 2015).

Apamin infusion significantly increased the number of phospho-ERK (pERK)-positive cells (vehicle, 4% ± 2%, n = 11; apamin, 13% ± 2%, n = 10; $p < 0.01$; Figures 5B and S5A) and pS6-positive cells in 6-OHDA-lesioned mice (vehicle, 28% ± 3%, n = 11; apamin, 47% ± 4%, n = 10; $p < 0.001$; Figures 5B and S5A). To determine the cell-type specificity of this effect, we infused apamin in the ipsilateral DLS of drd1a-tdTomato^{tg}/drd2-EGFP^{tg} 6-OHDA-lesioned animals. The number of pERK- and pS6-positive D1$_{MSN}$ increased with apamin (pERK, vehicle, 5% ± 2%, n = 8; apamin, 17% ± 5%, n = 9; $p < 0.01$; pS6, vehicle, 7% ± 1%, n = 8; apamin, 27% ± 5%, n = 9; $p < 0.01$; Figures 5C and S5B). In contrast, almost no pERK-positive D2$_{MSN}$ were detectable in either vehicle- or apamin-treated mice (vehicle, 0.1% ± 0.1%, n = 8; apamin, 0.2% ± 0.1%, n = 9; $p < 0.05$; Figures 5C and S5B), nor were there any differences in the number of pS6-positive D2$_{MSN}$ upon apamin infusion (vehicle, 39% ± 6%, n = 8; apamin, 46% ± 4%, n = 9; $p > 0.05$; Figures 5C and S5B). The number of pS6-positive cells appeared to directly correlate with the number of pERK-positive cells specifically in the D1$_{MSN}$ subpopulation (Figure 5C), consistent with previous observations (Bonito-Oliva et al., 2013).

Overall, these results demonstrate that inhibition of striatal SK channel activity selectively activates the ERK signaling cascade in D1$_{MSN}$.

Activating eCB and ERK Signaling In Vivo Alleviates Motor Abnormalities in PD Model Mice

Reminiscent of dopamine regulation, inhibition of SK channel activity results in distinct synaptic modulation of striatal pathways

in PD model mice. That is, SK channel inhibition rescues LTD in $D2_{MSN}$ by boosting the eCB system, while counteracting LTD in $D1_{MSN}$ by promoting the activation of postsynaptic ERK signaling. If these synaptic effects are directly related to motor behavior, inhibiting SK channel activity in the ipsilateral DLS of 6-OHDA mice in vivo should rescue some of the motor deficits. To test this, we assessed the impact of a single in vivo apamin infusion in the DLS on distinct forms of motor behaviors in PD mice.

In Vivo Inhibition of Striatal SK Channel Activity Reduces Asymmetric Motor Behavior and Enhances Motor Responses Induced by D1-Dopaminergic Drugs

In the unilateral 6-OHDA-lesioned mouse model, asymmetric dopamine depletion results in ipsiversive spontaneous rotations of the body and drug-induced contralateral rotations that are widely used to assess the effectiveness of treatment strategy (Schwarting and Huston, 1996). We tested whether rescuing the regulation of corticostriatal synapses (by inhibiting SK channels with apamin) could reduce the number of net ipsilateral rotations or potentiate contraversive turning behavior upon co-administration with dopaminergic agonists.

In vivo infusion of apamin in the ipsilateral DLS (0.08 ng/0.5 μl i.c.) indeed significantly reduced net ipsiversive spontaneous rotations of 6-OHDA-lesioned mice ($p < 0.001$, t test; Figure 6A). We then assessed whether this behavioral rescue by SK channel inhibition was directly linked to eCB or ERK signaling. We first measured the number of spontaneous rotations upon infusing apamin and apamin plus the CB1R antagonist AM251 (0.5 ng/0.5 μl i.c.). Manipulating the eCB system did not change the rescuing effect of apamin ($p > 0.05$, Tukey; Figure 6B) and had no effect alone ($p > 0.05$; Figure 6B). In contrast, co-injection of apamin with the MEK/ERK inhibitor PD0325901 (5 pg/0.5 μl i.c.) fully prevented the rescuing effect of apamin ($p < 0.001$, Tukey; Figure 6C). PD0325901 alone did not alter rotational behavior ($p > 0.05$, Tukey; Figure 6C).

Finally, we tested whether A1R antagonism, which similar to apamin prevents LTD in $D1_{MSN}$ (Figure 3C), affected the number of net ipsilateral rotations in the PD model. Alone, the A1R antagonist DPCPX (0.07 ng/0.5 μl i.c.) indeed recapitulated the behavioral effect of apamin ($p < 0.05$, Tukey; Figure 6D). Co-injecting apamin with DPCPX did not further increase the number of contraversive movements ($p > 0.05$, Tukey; Figure 6D). Net spontaneous locomotor activity was similar in the different cohorts of mice (Figures S6A and S6B).

We also evaluated the effect of apamin on contraversive turning behavior in response to a systemic low dose of the non-selective D1/D2 agonist apomorphine (0.1 mg/kg subcutaneously [s.c.]; Figure 6E). Apamin injection increased the number of apomorphine-induced rotations compared to vehicle-injected mice ($p < 0.05$, Tukey; Figure 6E). Apamin had no effect on contralateral rotations induced by administration of the selective D2 agonist pramipexole (1 mg/kg intraperitoneally [i.p.]; $p > 0.05$, Tukey; Figure S6C). In contrast, apamin did potentiate contralateral rotations induced by systemic administration of the selective D1 receptor agonist SKF38393 (SKF, 10 mg/kg i.p; $p < 0.05$, Tukey; Figure 6F). This effect was not mediated by the activation of CB1R, as it was insensitive to the co-injection of apamin with AM251 (0.5 ng/0.5 μl i.c.; $p < 0.05$, Tukey; Figure 6F).

Together, these results suggest that the rescue effect of modulating SK channels on turning behavior may occur through $D1_{MSN}$ activity, via the ERK-dependent counteraction of A1R-mediated LTD.

In Vivo SK Channel Inhibition in the DLS Improves Skilled Motor Deficits

We next evaluated the effects of in vivo SK channel inhibition on skilled motor behavior, which requires repetitive training paradigms for motor learning and fine movement control (Costa et al., 2004). First, we tested the duration of the inhibitory effect of a single apamin infusion in the DLS on the SK-mediated current (Figure S7). We found that apamin's effect lasted at least 24 hr (Figures S7A and S7B).

The motor abilities of 6-OHDA- and sham-lesioned mice were assessed by fixed-speed (FSRR) and accelerated (ARR) rotarod tests (Monville et al., 2006). In FSRR (15 rpm, 120 s maximum time), performances were significantly reduced in 6-OHDA mice compared to sham animals (6-OHDA, 57 ± 3 s; sham, 111 ± 2 s; $p < 0.001$, t test; Figures 7A and 7B). Apamin infusion improved motor performance of 6-OHDA-lesioned mice when tested 1, 24, and 48 hr after the injection ($p < 0.01$, Tukey; Figure 7A). Injection with vehicle had no effect on performance ($p > 0.05$; Figure 7A).

The effect of apamin was prevented by the CB1R antagonist AM251 (0.5 ng/0.5 μl i.c.; $p > 0.05$, Tukey; Figure 7A), which alone had no behavioral effect ($p > 0.05$, Tukey; Figure 7A). Collectively, mice receiving apamin had a significantly improved FSRR performance compared to the other groups (2WRM, Holm-Sidak: treatment, $F_{3,75} = 4.7$, $p = 0.0045$; session, $F_{2,150} = 0.09$, $p = 0.9$; session × treatment, $F_{6,150} = 1.8$, $p = 0.09$). Consistent with the duration of the in vivo inhibitory effect of apamin on SK channel activity (Figures S7A and S7B), we observed a significant motor improvement for up to 24 hr after drug infusion. After 7 days, performance on the rotarod no longer varied among groups (latency to fall, Veh_Veh, 56 ± 8 s, n = 22; APA_Veh, 63 ± 9 s, n = 24; APA_AM251, 51 ± 10 s, n = 16; Veh_AM251, 53 ± 10 s, n = 17; $p > 0.05$; data not shown). The pharmacological treatments had no behavioral effects in sham-lesioned animals (2WRM, Holm-Sidak: treatment, $F_{3,40} = 1.4$, $p = 0.3$; session, $F_{2,80} = 0.8$, $p = 0.4$; treatment × session, $F_{6,80} = 0.7$, $p = 0.6$; Figure 7B).

In vivo apamin infusion had a similar rescuing effect in the ARR test (4–40 rpm, 0.12 rpm/s, 300 s). 6-OHDA-lesioned mice, but not sham animals, showed improved motor performance upon apamin injection, and this was CB1R mediated (2WRM, Holm-Sidak: 6-OHDA, treatment, $F_{3,70} = 3.2$, $p = 0.03$; session, $F_{2,140} = 1.14$, $p = 0.32$; treatment × session, $F_{6,140} = 0.9$, $p = 0.5$; and sham, treatment, $F_{3,39} = 0.3$, $p = 0.8$; session, $F_{2,78} = 0.8$, $p = 0.5$; treatment × session, $F_{6,78} = 0.6$, $p = 0.8$; Figure S7C).

These results suggest that in vivo inhibition of SK channel activity improves skilled motor behavior through an eCB-mediated mechanism. To confirm this, we repeated the behavioral tests while co-injecting apamin and the PLD inhibitor CAY10594 (CAY, 22 ng/0.5 μl i.c.), which abolishes eCB plasticity at cortico-$D2_{MSN}$ synapses (Figure 2A). Inhibiting the activity of PLD prevented the rescuing effects of SK channel inhibition (2WRM, Holm-Sidak: FSRR, treatment, $F_{3,72} = 3.9$, $p < 0.05$;

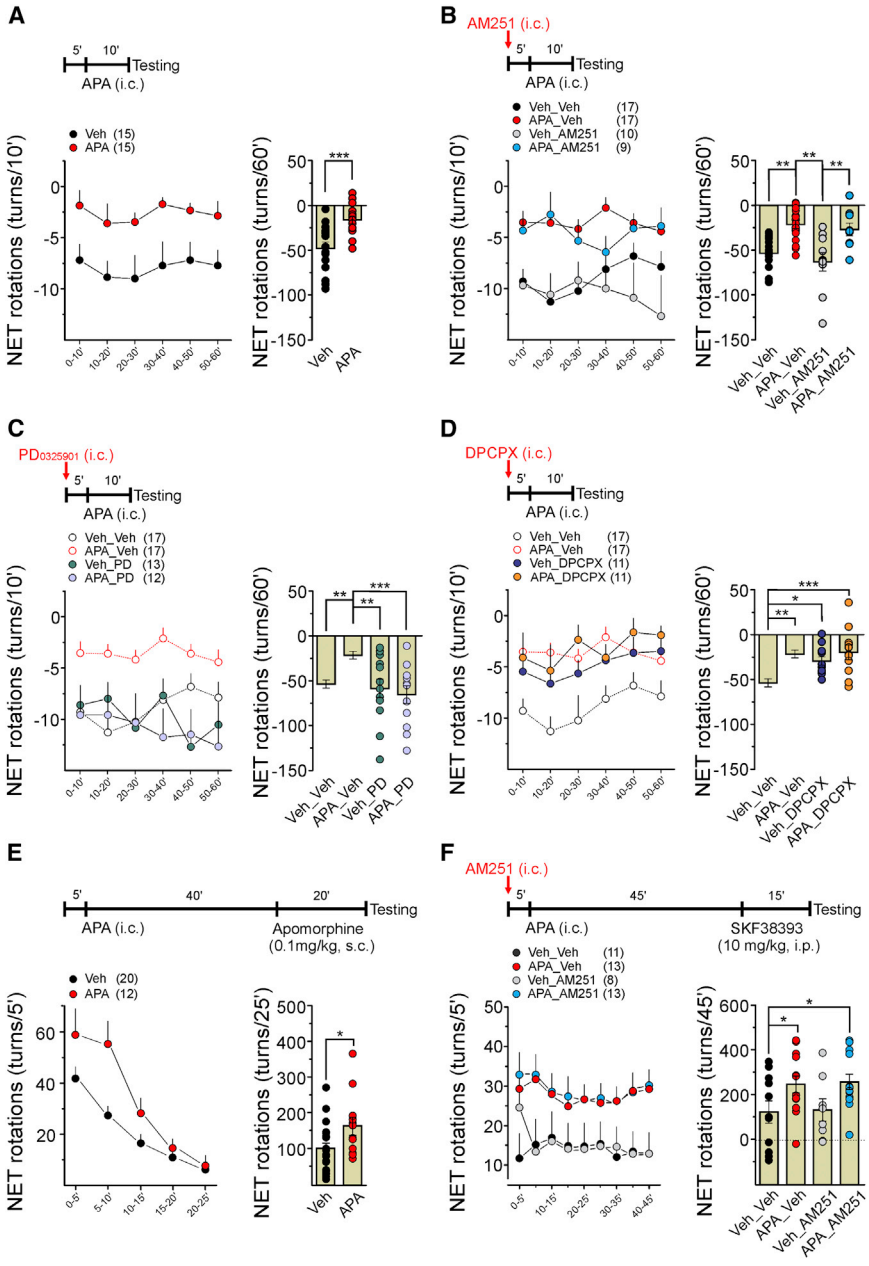

Figure 6. Effect of In Vivo Modulation of SK Channel Activity in the DLS of 6-OHDA-Lesioned Mice on Rotational Behavior

(A–D) (Top) Schematic of the pharmacological regimen of DLS injections (i.c.) and behavioral tests. (Bottom) Time courses (left) of spontaneous turning behavior computed every 10 min for 60 min and bar diagram (right) of net averaged rotations (contralateral-ipsilateral tight 180° rotations of the body) under the different pharmacological treatments are shown. Turns in the direction contralateral to the lesion are indicated by positive figures on the y axis.

(A) Spontaneous net ipsilateral rotations in 6-OHDA-lesioned mice upon apamin or vehicle infusion in the DLS are shown (APA, −16 ± 4, n = 15; vehicle −48 ± 7, n = 15).

(B) Behavioral effect of co-injection of apamin with the CB1R antagonist AM251, AM251 alone, or their vehicles is shown (APA_Veh, −21 ± 4, n = 17; Veh_Veh, −54 ± 4, n = 17; APA_AM251, −27 ± 7, n = 9; Veh_AM251, −63 ± 10, n = 10).

(C and D) The time courses (left) and 60 min-binning (right, bar diagrams) of spontaneous turning behavior from mice infused with vehicle or with apamin displayed in (B) are reported in (C) and (D) for comparison. (C) Behavioral effect of co-injection of apamin with PD0325901, PD032590 alone, or their vehicles is shown (APA_PD, −65 ± 10, n = 12; Veh_PD, −58 ± 10, n = 13). (D) Spontaneous net ipsilateral rotations in 6-OHDA-lesioned mice following a single injection of the A1R antagonist DPCPX or co-injection of DPCPX with apamin (Veh_DPCPX, −29 ± 5, n = 11; APA_DPCPX, −19 ± 8, n = 11).

(E and F) (Top) Order of pharmacological regimen of apamin injection (i.c.), administration of apomorphine (i.p.) (E) or SKF38393 (i.p.) (F), AM251 infusion (i.c.) (F), and behavioral tests. (Bottom) Time course (left) of motor activation computed every 5 min for 25 min (E) or every 5 min for 45 min (F) and bar diagram (right) of net averaged rotations are shown. (E) Effect of apamin infusion on apomorphine-induced contralateral rotations is shown (contralateral-ipsilateral tight 360° rotations of the body, vehicle, 103 ± 15, n = 20; APA, 165 ± 25, n = 12, $p < 0.05$). (F) SKF-induced contraversive rotations upon apamin and/or AM251 infusion are shown (Veh_Veh, 124 ± 50, n = 11; APA_Veh, 248 ± 38, n = 13; Veh_AM251, 134 ± 50, n = 8; APA_AM251, 259 ± 34, n = 13).

***$p < 0.001$, **$p < 0.01$, *$p < 0.05$.

session, $F_{2,144} = 2.9$, $p = 0.06$; treatment × session, $F_{6,144} = 0.9$, $p = 0.5$; and ARR, treatment, $F_{3,72} = 3.0$, $p < 0.05$; session, $F_{2,144} = 1.7$, $p = 0.2$; treatment × session, $F_{6,144} = 0.7$, $p = 0.7$; Figures S7D and S7E). Spontaneous locomotor activity was unchanged in 6-OHDA- and sham-lesioned mice when tested 1, 24, and 48 hr after drug infusion (Figures S7F and S7G).

Our results show that synaptic eCB signaling is required to gate LTD at cortical connections to $D2_{MSN}$ (Figure 1B), impaired upon dopaminergic denervation (Figure 4A) and reinstated at these specific synapses following inhibition of SK channel activity (Figure 4C), suggesting that eCB-LTD in $D2_{MSN}$ plays a critical role in producing coordinated behavior.

We cannot exclude, however, that the ERK-mediated increase in synaptic responsiveness of $D1_{MSN}$ with apamin (Figures 4D and 5) could contribute to improving motor performance of PD mice on the rotarod by alleviating the ipsilateral bias of motion (Figure 6). Indeed, in the FSRR test, the effect of apamin (2WRM, Holm-Sidak: treatment, $F_{3,66} = 5$, $p = 0.003$; session, $F_{2,132} = 1$, $p = 0.3$; session × treatment, $F_{6,132} = 2$, $p = 0.06$) was dampened by the co-injection of PD0325901 (5 pg/0.5 μl i.c; $p < 0.05$ at 1 hr; Figure 7C). These results indicate that apamin improves the rotarod performance of PD mice through a mechanism involving the concurrent activation of the eCB system and the ERK

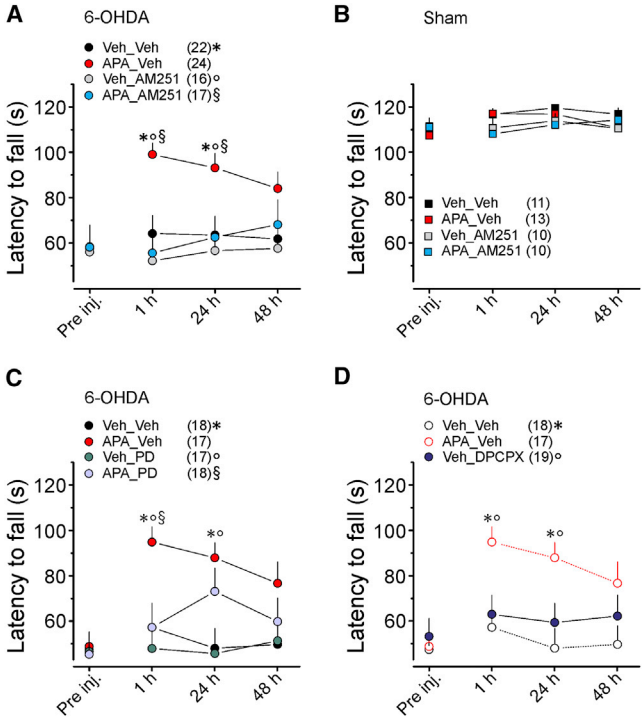

Figure 7. Effect of In Vivo Modulation of SK Channel Activity in the DLS on Skilled Motor Performance

(A) Performance of 6-OHDA-lesioned mice subjected to a fixed speed (15 rpm) rotarod test (FSRR) following intracerebral injection of apamin ($p < 0.01$). The effect of apamin was prevented by co-administration of the CB1R antagonist AM251 ($p > 0.05$). No changes in performance were observed in mice injected with saline ($p > 0.05$) or with AM251 ($p > 0.05$).

(B) No changes in rotarod performance were observed in the different cohorts of sham-lesioned mice ($p > 0.05$).

(C) Skilled motor performance of 6-OHDA-lesioned mice in the FSRR test upon a single infusion of the MEK/ERK inhibitor PD0325901, applied in isolation ($p > 0.05$) or co-injected with apamin, is shown ($p = 0.04$).

(D) Performance of 6-OHDA-lesioned mice in the FSRR test upon a single infusion of the A1R antagonist DPCPX ($p > 0.05$). Performance of 6-OHDA-lesioned mice infused with saline/DMSO or with apamin and displayed in (C) is reported here for comparison (dotted lines).

*, °, §$p < 0.05$ versus APA_Veh (RM1W, Tukey).

cascade. If this is the case, we would expect that mimicking the synaptic effect of ERK activation in $D1_{MSN}$ by exclusively blocking A1R should not be sufficient to improve skilled motor behavior. Consistent with this, we found that 6-OHDA-lesioned mice infused with DPCPX alone (0.07 ng/0.5 μl i.c., Veh_DPCPX) did not improve their motor abilities; they performed significantly worse than mice receiving apamin (2WRM, Holm-Sidak: FSRR, treatment, $F_{2,51} = 6$, $p = 0.006$; session, $F_{2,102} = 3$, $p = 0.08$; session × treatment, $F_{4,102} = 1$, $p = 0.4$; Veh_DPCPX versus Veh_Veh, $p > 0.05$; Veh_DPCPX versus APA_Veh, $p < 0.05$, at 1–24 hr; Figure 7D). Neither PD0325901 nor DPCPX affected spontaneous locomotor activity (Figure S7H).

Taken together, our data suggest that coordinated eCB and ERK signaling is required to enabling fine movement control during skilled motor behavior.

DISCUSSION

This study demonstrates that, in an experimental model of PD, the concomitant and cell-type-specific activation of the eCB and ERK signaling cascades in the DLS normalizes striatal circuitry and restores effective control of motor functions. These cascades can be activated by the manipulation of SK channel activity, which modulates eCB-LTD in $D2_{MSN}$ and adenosine-mediated LTD in $D1_{MSN}$. Our results are, therefore, consistent with a model in which the synaptic neuromodulators dopamine, eCBs, and adenosine are integrated and shape motor behavior by concurrently regulating mechanisms of synaptic plasticity in both MSN subpopulations.

HFS-LTD in $D2_{MSN}$ and $D1_{MSN}$

HFS of cortical afferents to the DLS induces LTD in both MSN subpopulations. In contrast to LTD at cortical connections to $D2_{MSN}$, the gating of HFS-LTD at $D1_{MSN}$ is independent of the activation of eCB and D2R signaling and unaffected by dopamine denervation. In this context, our results inform the still-debated issue of whether eCB-LTD is equally inducible in both $D2_{MSN}$ and $D1_{MSN}$ (Adermark and Lovinger, 2007; Bagetta et al., 2011; Kreitzer and Malenka, 2007; Nazzaro et al., 2012; Shen et al., 2008; Wang et al., 2006).

There is a general consensus that eCB-LTD can be reliably induced at glutamatergic synapses on identified $D2_{MSN}$ independently of the experimental paradigm (Adermark and Lovinger, 2007; Wang et al., 2006). In identified $D1_{MSN}$, HFS-LTD is not inducible using intrastriatal stimulation (Kreitzer and Malenka, 2007). However, this observation is challenged by studies showing a form of LTD in $D1_{MSN}$ that is dependent on CB1 and D2 receptors (Adermark and Lovinger, 2007; Bagetta et al., 2011) and blocked following striatal dopamine denervation (Bagetta et al., 2011).

Results obtained when plasticity is evoked by intrastriatal stimulation and those gained in this study by cortical stimulation may not be directly comparable. Indeed, monoamines (dopamine and serotonin) and thalamic glutamate released upon intrastriatal stimulation might affect the direction of synaptic plasticity in $D1_{MSN}$ (Wu et al., 2015). This is likely not to be the case upon stimulation of cortical layer V (Fino et al., 2005). Moreover, the majority of the studies investigating striatal HFS-LTD have been performed by voltage-clamp recordings (Adermark and Lovinger, 2007; Kreitzer and Malenka, 2007; Wang et al., 2006), using intracellular solutions containing high Cs^+ and TEA^+ concentrations, thus blocking potassium conductance. These experimental conditions could prevent differential potassium channel activation in $D1_{MSN}$ and $D2_{MSN}$ during stimulation and, hence, possibly mask differences in the threshold for induction of synaptic plasticity between the two MSN subpopulations. We favor the idea that the threshold for eCB production could be higher in $D1_{MSN}$ than $D2_{MSN}$. Indeed, we found that when the biosynthesis of eCBs was facilitated by the pharmacological stimulation of mGlur1/5R signaling, cortico-$D1_{MSN}$ synapses expressed a form of CB1R-dependent LTD, consistent with recent observations (Wu et al., 2015). Thus, while eCB-LTD may not be cell-type specific per se, the threshold for the induction of this form of plasticity can be modulated in a cell-type-specific manner.

Adenosine-Mediated LTD at Cortico-$D1_{MSN}$ Synapses

One key question is which neuromodulatory mechanisms govern LTD at $D2_{MSN}$ and $D1_{MSN}$ in response to different activity patterns of convergent synaptic inputs and ultimately fine-tune motor control. We show that upon HFS of cortical afferents, eCB signaling governs LTD at $D2_{MSN}$, whereas adenosine governs LTD at $D1_{MSN}$. This role of adenosine at striatal circuits was previously unknown. The source of adenosine may be the postsynaptic MSN or it may originate from the catabolism of ATP co-released with glutamate from glial and glutamatergic terminals upon HFS (Pascual et al., 2005).

In our conditions, adenosine-mediated LTD appears to be specifically expressed at cortical connections to $D1_{MSN}$ and requires the activation of A1Rs. In the striatum, A1Rs are found at corticostriatal afferents, where they negatively modulate glutamatergic neurotransmission, and on the postsynaptic $D1_{MSN}$ (Ferré et al., 1997). Our data, that both HFS-LTD and pharmacological A1R-dependent LTD at $D1_{MSN}$ show a presynaptic locus of expression, support a central role for presynaptic A1R in the induction of LTD at cortico-$D1_{MSN}$ synapses. We cannot exclude, however, that activation of postsynaptic A1R might be involved in the modulation of this form of plasticity through direct antagonism of D1R. In striatal homogenates, A1R inhibits the D1R-induced activation of adenylyl cyclase, and this also may occur in $D1_{MSN}$ where A1R and D1R co-localize (Ferré et al., 1997). By dampening the D1R-mediated activation of Gs signaling pathways that shift plasticity toward potentiation (Lerner and Kreitzer, 2011), activation of postsynaptic A1R could synergize with presynaptic A1R, thus bolstering the expression of LTD at cortico-$D1_{MSN}$ synapses.

Behavioral Relevance of Cell-Type-Specific Regulation of Synaptic Mechanisms of Plasticity

We provide evidence that restoring the functional integration of presynaptic and postsynaptic mechanisms of plasticity in $D2_{MSN}$ and $D1_{MSN}$ directly improves motor behavior in a mouse model of PD. In PD mice, the inhibition of SK channels in the DLS rescued the disease-linked deficits in eCB-LTD in $D2_{MSN}$ neurons. The same treatment increased the synaptic responsiveness of $D1_{MSN}$ via postsynaptic ERK activation, thus counteracting A1R-LTD. Inhibiting SK channel activity in the DLS in vivo alleviated specific motor abnormalities, supporting that differential modulation of synaptic mechanisms of plasticity at striatal pathways affects behavior (Figure S9).

The synaptic and behavioral effects of the SK-mediated modulation of the ERK signaling cascade in $D1_{MSN}$ of PD mice are fundamental points of novelty in our findings. The Ras-ERK signaling cascade is regulated by upstream neuron-specific guanine nucleotide exchange factors, including the Ca^{2+}-dependent exchange factor Ras-GRF1, which promotes the induction of LTP at corticostriatal synapses in $D1_{MSN}$, but not in $D2_{MSN}$ (Cerovic et al., 2015). Fine-tuning intracellular Ca^{2+} in $D1_{MSN}$ by inhibiting SK channels might promote ERK signaling activation via RasGRF1.

We show that in vivo inhibition of SK channels with apamin in the DLS of PD mice is sufficient to reduce pathological asymmetric turning behavior. Inhibiting the ERK cascade prevents this rescue. Furthermore, in vivo antagonism of A1R, which has a similar effect to apamin on LTD in $D1_{MSN}$, also recapitulates the effects of apamin on behavior. Apamin also enhances motor responses to the selective D1 agonist SKF38393 in the PD mouse model. Collectively, this evidence helps to build a model in which increasing the synaptic responsiveness of $D1_{MSN}$ rescues asymmetric turning behavior. In the PD state, characterized by striatopallidal hyperactivity and striatonigral hypoactivity (DeLong and Wichmann, 2009), the SK-mediated modulation of $D1_{MSN}$ may equilibrate the coordinated outputs of the two projection pathways to produce spontaneous contraversive movements (Tecuapetla et al., 2014).

In vivo administration of apamin in the DLS improves skilled motor behavior through a mechanism that requires intact eCB biosynthetic machinery and CB1R function. This strongly supports the direct relationship between eCB-LTD and this specific motor ability. Nevertheless, in vivo ERK antagonism dampens the rescuing effect of apamin. This suggests that coordinated eCB and ERK signaling is required to enable fine movement control on the rotarod.

It has been reported previously that systemic co-administration of an eCB degradation inhibitor and a D2 agonist partially rescues motor deficits in PD mice (Kreitzer and Malenka, 2007). Here, apamin infusion in the DLS improves motor function and skilled motor learning in the PD mouse model, without the need for dopaminergic stimulation. The numerous dissimilarities in the animal models (acute bilateral versus chronic dopamine-depleted mice) and in the treatment (systemic versus local) may account for this difference. Additionally, in this work, modulation of SK channel activity in the DLS concurrently engages synaptic mechanisms of plasticity (i.e., eCB and ERK signaling) in both $D2_{MSN}$ and $D1_{MSN}$, whereas in Kreitzer and Malenka (2007) study only the striatopallidal pathway was targeted.

Recent work has demonstrated that $D1_{MSN}$ and $D2_{MSN}$ act simultaneously during action initiation (Cui et al., 2013), rather than sequentially starting and stopping movement, as previously inferred (Albin et al., 1989). In PD, which is characterized by deficits in initiating and terminating sequences of movements, dopamine depletion may affect the coordinated activity of specific neural ensembles that activate or inhibit individual cortical motor programs (Cui et al., 2013). Since SK channels open in response to elevation of intracellular Ca^{2+}, we propose that the SK-mediated feedback modulation of voltage-dependent Ca^{2+} influx is particularly effective at modifying behavior (Nazzaro et al., 2012; this study), as this modulation may preferentially occur when convergent cortical activity brings striatal neurons into depolarized up states. This may allow for regulation of cell-type-specific Ca^{2+}-dependent intracellular pathways, specifically in cortically entrained striatal synapses. In PD model mice, this might re-establish the correct processing of behavioral information from the cerebral cortex through the basal ganglia circuits. In this view, striatal SK channels represent a promising non-dopaminergic target to concurrently regulate striatopallidal and striatonigral circuitry in basal ganglia disorders.

EXPERIMENTAL PROCEDURES

All procedures involving animals were carried out in accordance with the Italian Ministry of Health's directives (D.lgs 26/2014) regulating animal research.

Dopaminergic Lesion

Mice were injected with 6-OHDA HBr (3.5 μg/μl) into the right medial forebrain bundle (MFB). Severity of dopamine denervation was estimated 9–14 days later by computing the number of ipsilateral over total spontaneous rotations of the body in 6-OHDA- and sham-lesioned mice. Only mice displaying a ratio of ipsilateral/total tight rotations >90% were considered for further experiments (mean ± SEM; 45 min; 6-OHDA, 99% ± 0.1%, n = 498; sham, 49% ± 1.4%, n = 70; 6-OHDA versus sham, $p < 0.001$, t test). The extent of the lesion was later assessed by analyzing tyrosine hydroxylase (TH) levels in the striatum with immunohistochemistry. Only lesions >80% were included in the analysis (mean ± SEM; 6-OHDA, 94.2% ± 0.3%, n = 498; sham, 1.7% ± 0.7%, n = 70; 6-OHDA versus sham, $p < 0.001$, t test).

Intrastriatal Drug Infusion

Drug solutions were infused i.c. (0.5 μl, 0.15 μl/min). In rotometry experiments, the animals were injected with vehicle in the contralateral DLS. Drugs used were as follows: apamin (0.08 ng dissolved in 0.9% saline), AM251 (0.5 ng in 0.2% DMSO in saline), CAY10594 (22 ng in 0.2% DMSO in saline), PD0325901 (5 pg in 0.2% DMSO in saline), or DPCPX (0.07 ng in 0.2% DMSO in saline). Cannula placement for the various pharmacological experiments is shown in Figure S8.

Motor Behavior

Locomotor activity and rotational behavior were assessed by using the ANY-maze video tracking system (Stoelting). In rotarod experiments, behavioral training and testing took place on a TSE mouse RotaRod system (TSE Systems GmbH).

Electrophysiology

Horizontal slices (270 μm) were prepared as described previously (Nazzaro et al., 2012). Whole-cell current-clamp recordings in the DLS were conducted in potassium-methylsulfate-based internal solution (130 mM $KMeSO_4$, 5 mM KCl, 5 mM NaCl, 10 mM HEPES, 2 mM $MgCl_2$, 0.1 mM EGTA, 0.05 mM $CaCl_2$, 2 mM Na_2ATP, and 0.4 mM Na_3GTP [pH 7.2–7.3, 280–290 mOsm/kg]). EPSPs were evoked by stimulation of the deep cortical layer 5 of the somatosensory cortex in the presence of the $GABA_A$ receptor antagonist gabazine (10 μM). During HFS-plasticity induction (4 × 1 s long 100-Hz trains, repeated every 10 s), the postsynaptic cell was depolarized from −80 to −50 mV. Paired-pulse facilitation (PPF) was elicited by twin cortical stimuli (100-ms interval).

Immunostaining

Mice were perfused with 4% paraformaldehyde (PFA, w/v) in phosphate buffer (0.1 M PB [pH 7.4]), and cryostat sections (30 μm) were processed for immunohistochemistry, immunofluorescence, or Nissl staining.

Measurement of Dopamine Depletion

Sections were blocked with Tris-buffered saline (0.3% Triton X-100 and 3% BSA) incubated in primary antibody against TH (1:700, Santa Cruz Biotechnology), followed by secondary antibody and DAB-based revelation (VECTASTAIN Elite ABC-Peroxidase Kit).

Assessment of ERK Pathway Activation

Coronal brain slices were incubated in rabbit polyclonal antibody against p-S6 (Ser235/236) or p44/42 MAPK (Erk1/2; Thr202/Tyr204; 1:200, Cell Signaling Technology) and mouse anti-NeuN antibody (1:500, Millipore) in PBS containing 0.1 mM NaF, 0.3% TX, and 4% normal goat serum, followed by Alexa-coupled secondary antibodies (1:1,000, Invitrogen). Images of the DLS (six fields/mouse) were acquired, and the number of pERK- and pS6-positive neurons was counted.

Identification of $D2_{MSN}$ and $D1_{MSN}$

During electrophysiology experiments, MSNs were filled with Neurobiotin (0.5 mg/ml) and slices were subsequently fixed with 4% PFA. Antigen retrieval (sodium citrate 50 mM, 30 min, 80°C) was performed, and the slices were incubated in primary antibodies (anti-A2A, 1:250, Enzo Biosciences; and anti-substance P, 1:200, Millipore, diluted in 0.1 M PB containing 0.3% [v/v] Triton X-100 and 0.02% NaN_3). Sections were then incubated in Alexa 568-conjugated streptavidin (1:5,000; Invitrogen) followed by secondary antibodies (Invitrogen).

Data Analysis

The occurrence and magnitude of synaptic plasticity was evaluated by comparing the normalized EPSP amplitudes from the last 5 min of baseline recordings with the corresponding values at 20–30 min after HFS (HFS-LTD) and 15–20 min and 30–35 from DHPG and ENBA application, respectively. LTD plots were generated by averaging the peak amplitude of individual EPSPs in 1-min bins. The CV for EPSP was calculated by the ratio of the SD and the mean EPSP amplitude (Fino et al., 2005).

Statistics

Data were analyzed by one-way repeated-measures ANOVA (RM1W) for comparisons within a group and by one-way ANOVA (1W) and two-way (2W) or two-way repeated-measures ANOVA (RM2W) for between-group comparisons (GraphPad Instat 3 software). Post hoc analyses (Tukey, Bonferroni, and Holm-Sidak multiple comparison tests) were only performed for ANOVAs that yielded significant main effects. For comparisons of two groups, an independent two-sample t test was used (GraphPad Instat 3 software). Statistical figures for RM1W and 1W are reported in Table S1.

For detailed methods, see the Supplemental Experimental Procedures.

SUPPLEMENTAL INFORMATION

Supplemental Information includes Supplemental Experimental Procedures, nine figures, and one table and can be found with this article online at http://dx.doi.org/10.1016/j.celrep.2015.10.009.

AUTHOR CONTRIBUTIONS

M.T. designed and performed the behavioral and histochemical experiments and conducted animal surgeries. A.C. designed and conducted electrophysiological experiments. M.G. performed imaging experiments. C.N. and P.P.S. performed preliminary electrophysiological recordings. B.G. carried out preliminary rotametry experiments. M.C. and I.M. obtained the preliminary histochemical data. R.B. supervised M.C. and I.M. M.T., A.C., and R.B. contributed to critical reading of the manuscript. R.T. supervised the project, designed and directed the experiments, and wrote the manuscript.

ACKNOWLEDGMENTS

We are grateful to Vincent Paget-Blanc for helping with immunohistochemistry analysis, to Mattia Pesce for technical assistance during imaging experiments, and to Paola Pedarzani for helpful discussion of the results. We also thank Stefania Fasano for the training she provided with stereotaxic surgery. This research was supported by the Fondazione Istituto Italiano di Tecnologia and by grants provided by Compagnia di San Paolo (to R.T.), Fondazione Cariplo (to R.T. and R.B.), and Ministero della Salute (to R.T.).

Received: September 27, 2014
Revised: July 26, 2015
Accepted: October 4, 2015
Published: November 5, 2015

REFERENCES

Adermark, L., and Lovinger, D.M. (2007). Combined activation of L-type Ca2+ channels and synaptic transmission is sufficient to induce striatal long-term depression. J. Neurosci. *27*, 6781–6787.

Albin, R.L., Young, A.B., and Penney, J.B. (1989). The functional anatomy of basal ganglia disorders. Trends Neurosci. *12*, 366–375.

Bagetta, V., Picconi, B., Marinucci, S., Sgobio, C., Pendolino, V., Ghiglieri, V., Fusco, F.R., Giampà, C., and Calabresi, P. (2011). Dopamine-dependent long-term depression is expressed in striatal spiny neurons of both direct and indirect pathways: implications for Parkinson's disease. J. Neurosci. *31*, 12513–12522.

Bloodgood, B.L., and Sabatini, B.L. (2008). Regulation of synaptic signalling by postsynaptic, non-glutamate receptor ion channels. J. Physiol. *586*, 1475–1480.

Bonito-Oliva, A., Pallottino, S., Bertran-Gonzalez, J., Girault, J.A., Valjent, E., and Fisone, G. (2013). Haloperidol promotes mTORC1-dependent phosphorylation of ribosomal protein S6 via dopamine- and cAMP-regulated phosphoprotein of 32 kDa and inhibition of protein phosphatase-1. Neuropharmacology *72*, 197–203.

Borycz, J., Pereira, M.F., Melani, A., Rodrigues, R.J., Köfalvi, A., Panlilio, L., Pedata, F., Goldberg, S.R., Cunha, R.A., and Ferré, S. (2007). Differential glutamate-dependent and glutamate-independent adenosine A1 receptor-mediated modulation of dopamine release in different striatal compartments. J. Neurochem. *101*, 355–363.

Cahill, E., Pascoli, V., Trifilieff, P., Savoldi, D., Kappès, V., Lüscher, C., Caboche, J., and Vanhoutte, P. (2014). D1R/GluN1 complexes in the striatum integrate dopamine and glutamate signalling to control synaptic plasticity and cocaine-induced responses. Mol. Psychiatry *19*, 1295–1304.

Calabresi, P., Pisani, A., Mercuri, N.B., and Bernardi, G. (1992). Long-term potentiation in the striatum is unmasked by removing the voltage-dependent magnesium block of NMDA receptor channels. Eur. J. Neurosci. *4*, 929–935.

Calabresi, P., Gubellini, P., Centonze, D., Picconi, B., Bernardi, G., Chergui, K., Svenningsson, P., Fienberg, A.A., and Greengard, P. (2000). Dopamine and cAMP-regulated phosphoprotein 32 kDa controls both striatal long-term depression and long-term potentiation, opposing forms of synaptic plasticity. J. Neurosci. *20*, 8443–8451.

Calabresi, P., Picconi, B., Tozzi, A., Ghiglieri, V., and Di Filippo, M. (2014). Direct and indirect pathways of basal ganglia: a critical reappraisal. Nat. Neurosci. *17*, 1022–1030.

Cerovic, M., d'Isa, R., Tonini, R., and Brambilla, R. (2013). Molecular and cellular mechanisms of dopamine-mediated behavioral plasticity in the striatum. Neurobiol. Learn. Mem. *105*, 63–80.

Cerovic, M., Bagetta, V., Pendolino, V., Ghiglieri, V., Fasano, S., Morella, I., Hardingham, N., Heuer, A., Papale, A., Marchisella, F., et al. (2015). Derangement of Ras-guanine nucleotide-releasing factor 1 (Ras-GRF1) and extracellular signal-regulated kinase (ERK) dependent striatal plasticity in L-DOPA-induced dyskinesia. Biol. Psychiatry *77*, 106–115.

Costa, R.M., Cohen, D., and Nicolelis, M.A. (2004). Differential corticostriatal plasticity during fast and slow motor skill learning in mice. Curr. Biol. *14*, 1124–1134.

Cui, G., Jun, S.B., Jin, X., Pham, M.D., Vogel, S.S., Lovinger, D.M., and Costa, R.M. (2013). Concurrent activation of striatal direct and indirect pathways during action initiation. Nature *494*, 238–242.

DeLong, M., and Wichmann, T. (2009). Update on models of basal ganglia function and dysfunction. Parkinsonism Relat. Disord. *15* (*Suppl 3*), S237–S240.

Ferré, S., Fredholm, B.B., Morelli, M., Popoli, P., and Fuxe, K. (1997). Adenosine-dopamine receptor-receptor interactions as an integrative mechanism in the basal ganglia. Trends Neurosci. *20*, 482–487.

Fino, E., Glowinski, J., and Venance, L. (2005). Bidirectional activity-dependent plasticity at corticostriatal synapses. J. Neurosci. *25*, 11279–11287.

Gerdeman, G.L., Ronesi, J., and Lovinger, D.M. (2002). Postsynaptic endocannabinoid release is critical to long-term depression in the striatum. Nat. Neurosci. *5*, 446–451.

Girault, J.A., Valjent, E., Caboche, J., and Hervé, D. (2007). ERK2: a logical AND gate critical for drug-induced plasticity? Curr. Opin. Pharmacol. *7*, 77–85.

Kreitzer, A.C. (2009). Physiology and pharmacology of striatal neurons. Annu. Rev. Neurosci. *32*, 127–147.

Kreitzer, A.C., and Malenka, R.C. (2007). Endocannabinoid-mediated rescue of striatal LTD and motor deficits in Parkinson's disease models. Nature *445*, 643–647.

Kupferschmidt, D.A., and Lovinger, D.M. (2015). Inhibition of presynaptic calcium transients in cortical inputs to the dorsolateral striatum by metabotropic GABA(B) and mGlu2/3 receptors. J. Physiol. *593*, 2295–2310.

Lerner, T.N., and Kreitzer, A.C. (2011). Neuromodulatory control of striatal plasticity and behavior. Curr. Opin. Neurobiol. *21*, 322–327.

Lerner, T.N., and Kreitzer, A.C. (2012). RGS4 is required for dopaminergic control of striatal LTD and susceptibility to parkinsonian motor deficits. Neuron *73*, 347–359.

Min, R., and Nevian, T. (2012). Astrocyte signaling controls spike timing-dependent depression at neocortical synapses. Nat. Neurosci. *15*, 746–753.

Monville, C., Torres, E.M., and Dunnett, S.B. (2006). Comparison of incremental and accelerating protocols of the rotarod test for the assessment of motor deficits in the 6-OHDA model. J. Neurosci. Methods *158*, 219–223.

Nazzaro, C., Greco, B., Cerovic, M., Baxter, P., Rubino, T., Trusel, M., Parolaro, D., Tkatch, T., Benfenati, F., Pedarzani, P., and Tonini, R. (2012). SK channel modulation rescues striatal plasticity and control over habit in cannabinoid tolerance. Nat. Neurosci. *15*, 284–293.

Packard, M.G., and Knowlton, B.J. (2002). Learning and memory functions of the Basal Ganglia. Annu. Rev. Neurosci. *25*, 563–593.

Pascoli, V., Turiault, M., and Lüscher, C. (2012). Reversal of cocaine-evoked synaptic potentiation resets drug-induced adaptive behaviour. Nature *481*, 71–75.

Pascual, O., Casper, K.B., Kubera, C., Zhang, J., Revilla-Sanchez, R., Sul, J.Y., Takano, H., Moss, S.J., McCarthy, K., and Haydon, P.G. (2005). Astrocytic purinergic signaling coordinates synaptic networks. Science *310*, 113–116.

Picconi, B., Centonze, D., Håkansson, K., Bernardi, G., Greengard, P., Fisone, G., Cenci, M.A., and Calabresi, P. (2003). Loss of bidirectional striatal synaptic plasticity in L-DOPA-induced dyskinesia. Nat. Neurosci. *6*, 501–506.

Schwarting, R.K., and Huston, J.P. (1996). The unilateral 6-hydroxydopamine lesion model in behavioral brain research. Analysis of functional deficits, recovery and treatments. Prog. Neurobiol. *50*, 275–331.

Shen, W., Flajolet, M., Greengard, P., and Surmeier, D.J. (2008). Dichotomous dopaminergic control of striatal synaptic plasticity. Science *321*, 848–851.

Tecuapetla, F., Matias, S., Dugue, G.P., Mainen, Z.F., and Costa, R.M. (2014). Balanced activity in basal ganglia projection pathways is critical for contraversive movements. Nat. Commun. *5*, 4315.

Tonini, R., Ferraro, T., Sampedro-Castañeda, M., Cavaccini, A., Stocker, M., Richards, C.D., and Pedarzani, P. (2013). Small-conductance Ca2+-activated K+ channels modulate action potential-induced Ca2+ transients in hippocampal neurons. J. Neurophysiol. *109*, 1514–1524.

Tritsch, N.X., and Sabatini, B.L. (2012). Dopaminergic modulation of synaptic transmission in cortex and striatum. Neuron *76*, 33–50.

Uchigashima, M., Narushima, M., Fukaya, M., Katona, I., Kano, M., and Watanabe, M. (2007). Subcellular arrangement of molecules for 2-arachidonoylglycerol-mediated retrograde signaling and its physiological contribution to synaptic modulation in the striatum. J. Neurosci. *27*, 3663–3676.

Wang, Z., Kai, L., Day, M., Ronesi, J., Yin, H.H., Ding, J., Tkatch, T., Lovinger, D.M., and Surmeier, D.J. (2006). Dopaminergic control of corticostriatal long-term synaptic depression in medium spiny neurons is mediated by cholinergic interneurons. Neuron *50*, 443–452.

Wu, Y.W., Kim, J.I., Tawfik, V.L., Lalchandani, R.R., Scherrer, G., and Ding, J.B. (2015). Input- and cell-type-specific endocannabinoid-dependent LTD in the striatum. Cell Rep. *10*, 75–87.